Thermal Properties of Lithium–Ion Battery and Components

Hossein Maleki, Said Al Hallaj, J. Robert Selman, Ralph B. Dinwiddie and H. Wang

J. Electrochem. Soc. 1999, Volume 146, Issue 3, Pages 947-954.
doi: 10.1149/1.1391704

Journal of The Electrochemical Society, **146** (3) 947-954 (1999)
S0013-4651(98)06-095-9 CCC: $7.00 © The Electrochemical Society, Inc.

Thermal Properties of Lithium-Ion Battery and Components

Hossein Maleki,[a,c] Said Al Hallaj,[*,a] J. Robert Selman,[,a] Ralph B. Dinwiddie,[b] and H. Wang[b]**

[a]*Center for Electrochemical Science and Engineering, Illinois Institute of Technology, Chicago, Illinois 60616, USA*
[b]*Oak Ridge National Laboratory, Metals and Ceramics Division, Oak Ridge, Tennessee 37831-6064, USA*

Experimental thermal property data of the Sony US-18650 lithium-ion battery and components are presented, as well as thermal property measuring techniques. The properties in question are specific heat capacity (C_p), thermal diffusivity (α), and thermal conductivity (k), in the presence and absence of electrolyte [1 M $LiPF_6$ in ethylene carbonate-dimethyl carbonate (EC:DMC, 1:1 wt %)]: The heat capacity of the battery, C_p, is 0.96 ± 0.02 J g^{-1} K^{-1} at an open-circuit voltage (*OCV*) of 2.75 V, and 1.04 ± 0.02 J g^{-1} K^{-1} at 3.75 V. The thermal conductivity, k, was calculated from $k \equiv \alpha\rho C_p$ where α was measured by a xenon-flash technique. In the absence of electrolyte, k increases with *OCV*, for both the negative electrode (NE) and the positive electrode (PE). For the NE, the increase is 26% as the *OCV* increases from 2.75 to 3.75 V, whereas for the PE the increase is only 5 to 6%. The dependence of both C_p and k on *OCV* is explained qualitatively by considering the effect of lithiation and delithiation on the electron carrier density, which leads to n-type semiconduction in the graphitic NE material, but a change from semiconducting to metallic character in Li_xCoO_2 PE material. The overall effect is an increase of C_p and k with *OCV*. For k this dependence is eliminated by electrolyte addition, which, however, greatly increases the effective k of the layered battery components by lowering the thermal contact resistance. For both NE and PE, the in-plane k value (measured along layers) is nearly one order of magnitude higher than the cross-plane k. This is ascribed mostly to the high thermal conductivity of the current collectors and to a lesser extent to the orientation of particles in the layers of electrodes.

Manuscript submitted April 15, 1998; revised manuscript received October 12, 1998.

A successful rechargeable lithium battery of high energy density has been developed based on shuttling of lithium ions between two intercalation electrodes ("rocking chair cell"). Commercially available lithium-ion cells have a negative electrode (NE) consisting of a copper foil coated with a mixture of carbon-based material, binder, and carbon black, an electrolyte consisting of lithium salts in organic solvent, and a positive electrode (PE) consisting of a mixture of lithium transition metal oxides, binder, and carbon black coated over aluminum foil. The separator (Sp) is a microporous polymer having good ionic and sufficiently low electronic conductivity, such as polypropylene. During charge, lithium ions deintercalate from the PE and intercalate into the NE, and the reverse takes place during discharge.

The operation of most lithium-ion cells is limited to a temperature range of 20 to 55°C, in which heat generation due to internal resistance and polarization is easily controllable by working within the voltage window (upper/lower cutoff voltage) and range of charge/discharge rates recommended by the manufacturers. Abuse conditions (high discharge/charge rates, short circuits, and operation at high ambient temperature) steeply accelerate the net accumulation of thermal energy in lithium-ion cells. The rate of heat generation increases exponentially with cell temperature, while the rate of heat transfer to a cool environment (ambient cooling) increases only linearly. Ultimately, the cell may experience "thermal runaway" accompanied by pressure buildup, which may lead to bursting of the cell, or fire. To guarantee a safe operation under any conditions, commercial lithium-ion cells are therefore of relatively small size.

For portable and mobile power applications, however, scaled-up batteries are desirable. For example, systems of 100 W/kg power density suitable for electric-vehicle applications are being developed.[9] A lithium-ion battery similar to the Sony type US-18650 cell, which is based on $Li_xC_6/Li_{1-x}CoO_2$ chemistry, might be suitable if its present capacity (1.37 Ah) could be increased by two orders of magnitude. To predict the thermal behavior of scaled-up designs of such batteries over a wide range of operating conditions, researchers use various models.[1-8] In principle, the analysis of such cells, especially if they are not elongated, requires two- or three-dimensional models. However, in practice, many one-dimensional "thermal" models are used. This may appear to be a reasonable simplification for a prismatic cell with stacked electrode layers, or a cylindrical cell having spirally wound layers, provided such cells of elongated geometry have a high aspect ratio (height/area or length/diameter).

However, for a more accurate check on the validity of the one-dimensional assumption, one must know the thermal conductivities of cell components in the direction of the electrode surface (in-plane k) as well as perpendicular to it (cross-plane k). Experimental values for these properties are not widely available in the literature; therefore, this work aims to present some methods of measurement and provides relevant data. The experiments are illustrated by application to the commercially available Sony US-18650 cylindrical lithium-ion cell, which has a nominal capacity of 1.35 Ah. The cell was retrieved from a double-battery pack used in Sony Camcorders, purchased in September, 1996, from the Sony Products Store in Chicago, IL 60616. This cell contains a NE which consists of specially tailored micrographitic carbon flakes as NE material and a highly layered structure $LiCoO_2$ as PE material. Based on the masses of the active PE and NE materials, recovered from current collectors coated on both sides, a loading ratio of about 1.89 was estimated for this cell. The exact amount of binder material and other additives included in both electrodes is unknown. The individual cell components were measured and weighted, with results shown in Table I.

Two different methods of measuring C_p were used: (*i*) transient temperature measurement and (*ii*) adiabatic calorimetry. Similarly, two methods were used to obtain k values for cell components. In the first method, the cross-plane k was determined by applying a known heat flux across the surface of PE/Sp/NE layers, and sampling the temperature difference at known locations between the stacked layers. In the second method, both cross-sectional and in-plane k values were calculated from cross-plane and in-plane thermal diffusivity ($\alpha \equiv k/\rho C_p$) measured by a xenon flash technique (XFT), with and without electrolyte [1 M $LiPF_6$ in EC-DMC (1:1 wt %)].

Experimental

Specific heat capacity, method 1 (cooling transient).—Figure 1 shows a schematic diagram of the heating assembly used to measure C_p of a Sony battery at *OCV* = 2.74 V. The core of this assembly was formed by an insulating cylindrical block of polystyrene foam (120 mm od, 150 mm long) with a closed-end cylindrical cavity (19 mm id, 100 mm deep). A high-resistance Ni/Cr heater (AWG 24, from Omega), electrically insulated by high-thermal-conductivity tape, spirally wound, was fitted close to the cavity wall. An Arbin battery cycler (Arbin Instrument Corporation, College Station, TX, model BT-2042) supplied direct current to the heater.

* Electrochemical Society Student Member.
** Electrochemical Society Active Member.
[c] Present address: Motorola, Energy Systems Group, Laurenceville, GA 30043.

S0013-4651(98)06-095-9 CCC: $7.00

Table I. Physical parameters of the Sony 18650 lithium-ion battery components.

Components	Positive electrode	Negative electrode	Separator
Total electrode mass, g	15.2	9.10	1.28
Total length, mm	521.1	534.0	1192.0
Total width, mm	52.9	56.0	59.2
Total thickness, mm	0.185	0.198	0.025
Foil thickness, mm	0.02	0.018	
Mass of active material, g	13.9	7.35	

The external heat-transfer coefficient (h, W m^{-2} K^{-1}), determining heat loss from the assembly, was measured using a type 416 stainless steel reference sample ($C_p \approx 04.56$ J g^{-1} K^{-1}), shaped to the geometry of the Sony battery (18 mm diam, 65 mm long). The reference sample was placed inside the heater cavity and heated to 60°C, slowly enough for the sample temperature to remain uniform. The power to the heater was then cut off, and the temperature (T) was sampled at 1 s intervals by two type E (Ni-Cr vs. Cu-Ni) thermocouples attached at opposite sides of the reference sample, at a location midway along its length. The ambient temperature (T_a) was monitored independently with a type E thermocouple positioned at a location 300 mm from the outside wall of the insulating block. Data sampling continued until the temperature difference (sample/ambient) was less than 1 K. Convection cooling was prevented by making the cavity fit the reference sample or cell closely.

An energy balance

$$\dot{Q}/hA\,(T - T_a) + mC_p[dT/dt] \qquad [1]$$

was used to calculate the external heat-transfer coefficient (h) of the assembly. Here, $\dot{Q}$ is the heat supplied by the heater, and the other symbols (see List of Symbols) refer to the sample. The solution to this equation is

$$\frac{T - T_a}{T_{ss} - T_a} = 1 - e^{-\tau} \quad \text{where} \quad \tau = \frac{t}{mC_p/hA} \quad \text{and}$$

$$T_{ss} = T_a + \dot{Q}/hA \qquad [2]$$

Here t is the time elapsed since the start of heating, and T_{ss} the temperature when the steady state is reached.

Since $\dot{Q} = 0$ during cooling, the solution to Eq. 1 becomes simply $\theta = \exp(-\tau)$, where τ is defined as above with t being the time elapsed since the start of cooling. Therefore, if the value of C_p is known, h can be obtained from mC_p/A times the negative slope of a plot of ln $(T - T_a)$ vs. time

$$h = -mC_p/A\; d/dt\; [\ln\{(T - T_a)/(Tss - T_a)\}] \qquad [3]$$

Figure 2a shows a plot of ln $(T - T_a)$ vs. cooling time for the reference sample, whose slope (-0.0008 s^{-1}), with $m = 152.7$ g, $C_p = 4.65$ J g^{-1} K^{-1}, and $A = 4.18 \times 10^{-3}$ m^2, yields $h = 13.45 \pm 0.1$ W m^{-2} K^{-1}. The same procedure applied to the Sony cell at $OCV = 2.75$ V (Fig. 2b), yields a slope (-0.00175 s^{-1}) from which, with the value $h = 13.43 \pm 0.1$ W m^{-2} K^{-1}, $m = 49$ g, and $A = 4.18 \times 10^{-3}$ m^2, as determined previously, the C_p of the Sony cell would be 0.800 J g^{-1} K^{-1}. To check this result, the value of C_p was determined directly, using adiabatic calorimetry.

Specific heat capacity, method two (adiabatic calorimetry).—Figure 3 shows a schematic diagram of the two-part adiabatic calorimeter used for measuring C_p. The lower part consists of a thin-walled cylindrical aluminum container (ca. 0.3 mm thick, 25 mm id, 100 mm long) partially filled with transformer oil and a heating coil. The container is surrounded by a Styrofoam and Dewar insulation assembly. The upper part of the calorimeter is used to preheat the reference sample or cell to be immersed, or to stabilize its temperature. It also contains a heater coil and is insulated by styrofoam. In the lower chamber, high thermal conductivity transformer oil (Midtown Petroleum Co., IL, L no. T-1026) is used for rapid dissipation of temperature differences in the calorimeter. Heating is provided by a Hewlett Packard-6632A dc power supply. A microvoltmeter

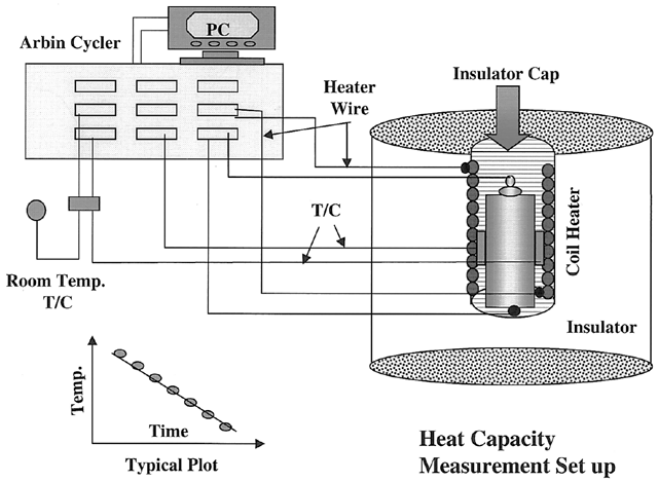

Figure 1. Detail of heat-flux calorimeter setup for measuring the specific heat capacity of the Sony US-18650 lithium-ion battery. Inset: typical plot of cooling profile for battery or reference sample.

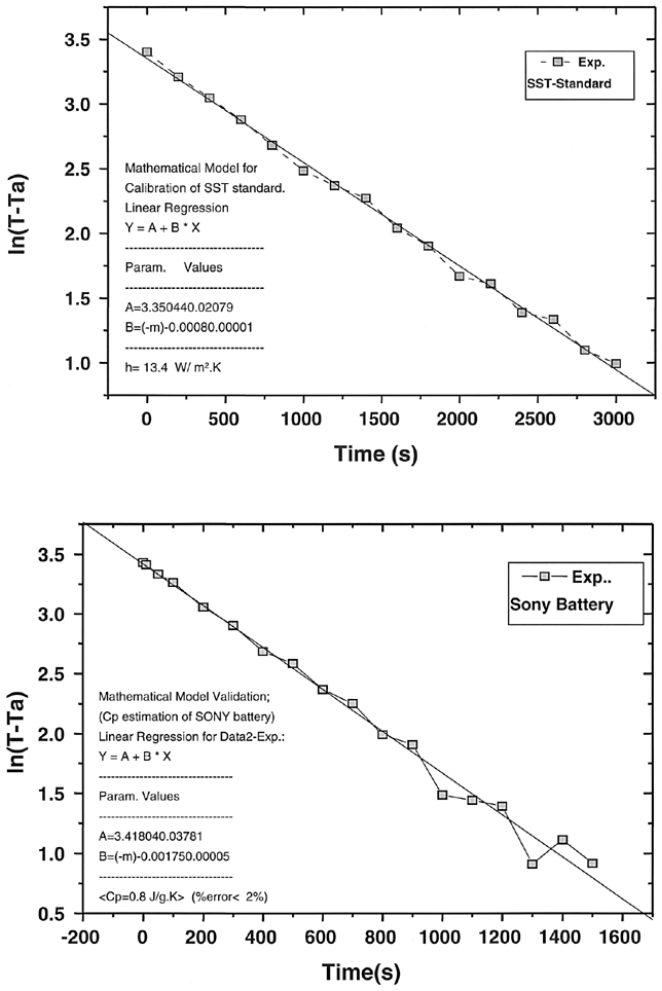

Figure 2. Cooling profiles of (a, top) stainless steel reference sample; (b, bottom) Sony US-18650 lithium-ion battery. Both are initially heated to 50°C.

S0013-4651(98)06-095-9 CCC: $7.00

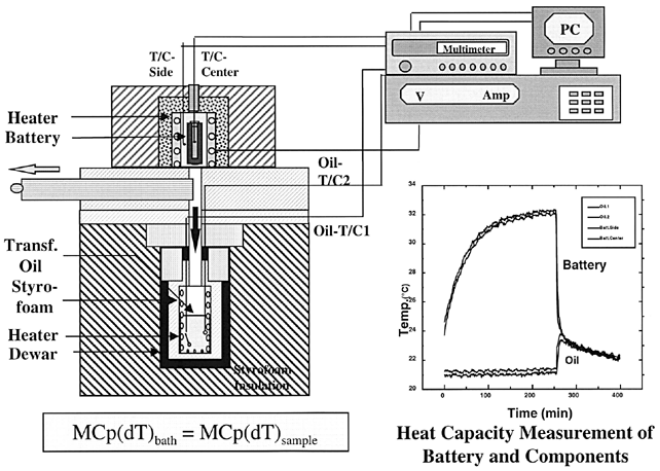

Figure 3. Schematic diagram of adiabatic calorimeter used to measure the specific heat capacity of the lithium-ion battery. Inset: Typical temperature vs. time profile.

(Keithley 2000, 10 channel multimeter) measures the temperatures of sample and oil bath simultaneously. The upper and lower chambers are separated by a sliding trap door made of Styrofoam. To immerse the reference sample or battery into the transformer oil of the lower chamber, the trap door is pulled out. A wire restrains the fall of the sample so as to avoid splashing.

The calorimeter constant, i.e., total heat capacity (K, J K^{-1}), was determined using a reference sample of aluminum or type 416 stainless steel, sized to the geometry of the Sony lithium-ion cell. The sample was placed in the upper insulation compartment of the calorimeter, but not heated, while the bath oil was heated to a temperature of 310 to 315 K. After the bath oil reached a stationary temperature (typically after 1 to 2 h), the reference sample or cell (still at room temperature) was immersed slowly. The final temperature of the lower chamber was measured after about 10 min. Figures 4a and b show typical temperature profiles for the aluminum reference sample and the Sony cell.

The calorimeter constant (K) was calculated from

$$K\,(\Delta T)_{\text{bath}} = (mC_{\text{p}}\Delta T)_{\text{bath}} = (mC_{\text{p}}\Delta T)_{\text{sample or battery}} \qquad [4]$$

The results are given in Table II, in chronological order. Apparently, changes (probably physical) occurred after the first three measurements. Since the time needed for heat conduction in aluminum is much shorter than in stainless steel, equilibrium is reached more rapidly, and the graphs (Fig. 4) are easier to read accurately. Hence the values based on the aluminum reference sample are probably more reliable. The last two of the values based on stainless steel agree with these. Therefore, the average over five independent aluminum

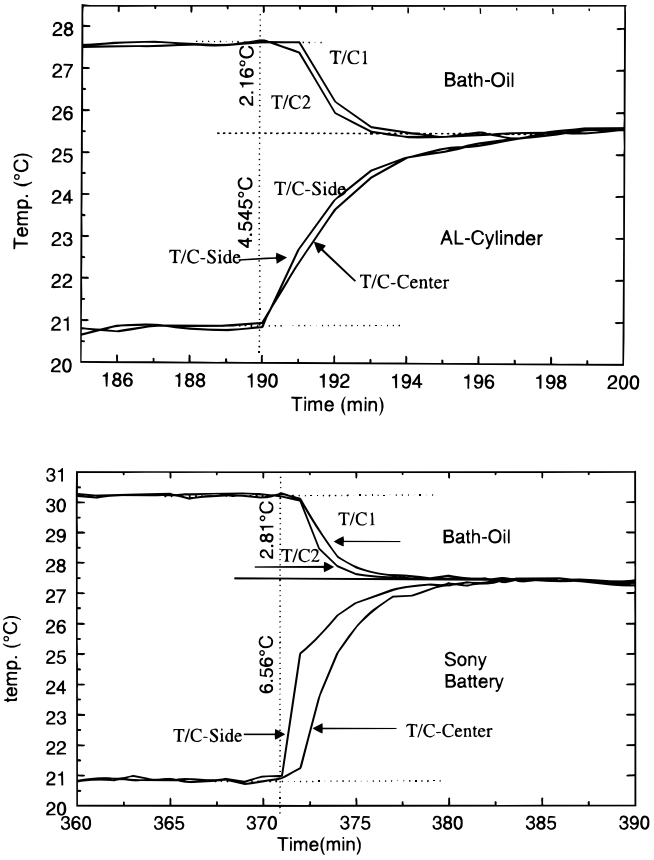

Figure 4. Typical profiles of temperature vs. time using (hot bath/room-temperature sample or battery) procedure, used for calculation of heat capacity: (a, top) sample and (b, bottom) battery.

standard measurements, conducted at 24 h apart, was used to calculate K.

To determine C_{p} of the Sony cell (C_{pbattery}), the hot bath oil/room-temperature sample procedure was adopted. The temperature difference cell/bath oil was monitored from the initial difference to thermal equilibrium, at 1/2 min intervals. C_{pbattery} was then calculated from Eq. 4.

Table III shows C_{pbattery} values measured in the range of room temperature to ca. 315 K. These values are higher than those obtained by the first method by about 20%. They also are closer to the values estimated[1-8] or measured by others.[9]

Thermal conductivity, method 1, direct steady-state measurement.—Figure 5 shows the experimental setup used to measure

Table II. Specific heat capacity of reference samples. C_{pAl}: specific heat capacity of aluminum reference sample from experimental measurements evaluated by using the averaged value of the calorimeter constant, K_{SS}, derived from measurements using a type 416 stainless steel sample. C_{pss}: specific heat capacity of type 416 stainless steel reference sample similarly evaluated using the averaged value of the calorimeter constant, K_{Al}, derived from measurements using an aluminum reference sample.

Calibration constant					
K_{SS}	K_{Al}	C_{pAl} vs. K_{SS} (J g^{-1} K^{-1})	Relative deviation	C_{pss} vs. K_{AL} (J g^{-1} K^{-1})	Relative deviation
112.30	96.71				
107.35	97.15	0.898	<1%	0.462	<1%
106.90	95.88	0.947	5.2%	0.461	—
98.52	92.90	0.877	2.5%	0.461	—
94.51	98.50	0.968	7.5%	0.462	—
103.91 ± 7%	96.20 ± 2%	C_{pav} = 0.92	4%	C_{pav} = 0.46	

CRC Handbook: C_{pAl} = 0.900 J/g/°C and C_{pss} − 416 = 0.460 J/g/°C.

S0013-4651(98)06-095-9 CCC: $7.00

Table III. Specific heat capacity of the Sony US-18650 lithium-ion battery at *OCV* = 3.75 V and *OCV* = 2.75 V. All experiments carried out using (hot bath/room-temperature cell) procedure.

Experiments	ΔT (Oil) (K)	ΔT (Batt.) (K)	K_{al} (J g^{-1})	C_p based on K_{Al} (J g^{-1} K^{-1})
OCV = 3.75 V	4.07	8.94	96.2	1.012
	3.39	6.38	96.2	1.088
	2.47	5.41	96.2	1.020
	2.63	5.70	96.2	1.036
				Average = 1.04 ± 0.034
OCV = 2.75 V	2.41	5.18	96.2	1.010
	2.54	6.25	96.2	0.909
	1.72	4.11	96.2	0.936
	2.02	4.67	96.2	0.967
	2.81	6.25	96.2	1.000
				Average = 0.96 ± 0.018

directly the thermal conductivity of composite stacked layers of the battery component PE, NE, or PE/Sp/NE layers stacked, using a heat flux perpendicular to the plane of the layers. Prior to thermal-conductivity measurements, conducted in open air with no electrolyte present, samples were washed in ethanol and dried at 60°C under argon atmosphere in a dry box. The heating assembly was a form of terminal resistor composed of high resistance Ni/Cr wire (AWG 28, from Omega) with a nickel strip spot-welded to each end. Each nickel strip was soldered to two stranded copper wires; one for current application and the other for potential measurement. Current was supplied by a dc power supply (Hewlett Packard 6642A), and voltage was measured by a Keithley model 2000 microvoltmeter. The heating wire, insulated by a thin-wall Teflon sleeve, was placed between two thin copper sheets (431 mm^2 and 0.18 mm thick).

Sample layers, each having an area comparable to that of the heater surface, were placed in contact with both sides of the heater assembly, with a thin flathead type E thermocouple inserted between them at selected locations, as shown in Fig. 5. High-thermal-conductivity paste (Omega lot no. 8411) was applied between sample layers, and layers were sandwiched between rectangular blocks of Styrofoam which also served as an enclosure. This assembly was placed in a two-part press with internal rims at top and bottom to apply pressure to the sample layers. To insure good thermal contact, the upper and lower halves of the Plexiglas press were compressed firmly at their four corners by means of through bolts. With stacked layers under compression and thermally insulated around the edges, the heat flow generated by the heater was directed perpendicular to the plane of the layers. The temperature was measured between layers.

A constant current (I) of 0.5, 1.0, or 1.5 A was supplied to the heater. For each current, five temperature measurements were carried out, and the voltage was measured at locations where the heater wire entered into the copper foil. The thermal conductivity (k) was then calculated using Eq. 5

$$k = (L_x/A)\,(I\,V/\Delta T_x) \qquad [5]$$

Here, ΔT_x is the temperature difference between the heater plate (read by thermocouple no. 1 in intimate contact with the copper plate) and the xth layer above the copper plate. V is the potential difference across the heater wire; I, the supplied current; L_x, the distance over which ΔT_x is measured; and A, the surface area of each of the sample layers.

The choice of insulation materials is important,[11] as well as the location of the thermocouples. The thickness of a single PE/Sp/NE assembly was ca. 0.42 mm. Thermocouple no. 1 was located at zero distance from the heater plate, thermocouples no. 2 to no. 5 at distances L_1 to L_4 from the surface of the heater plate, which closely corresponds to the accumulated thickness of successive layers. Thermocouples were flat tip (0.18 mm thick) type E (Omega Corp, Stamford, CT 06907).

The measured values of k range from 0.66 to 0.33 W m^{-1} K^{-1} depending on the current level and location where ΔT_x was measured. However, all values were lower than those calculated from data for lithium-ion battery components (PE, NE, and separator) given by Chen and Evans[3] and Kanari.[8] Because we felt that our direct thermal conductivity measurements at steady state might be affected by inevitable heat losses, we used a second dynamic method to check these k values.

Thermal conductivity, method 2, from thermal diffusivity measurement.—If the thermal diffusivity (α) of a stack of components is

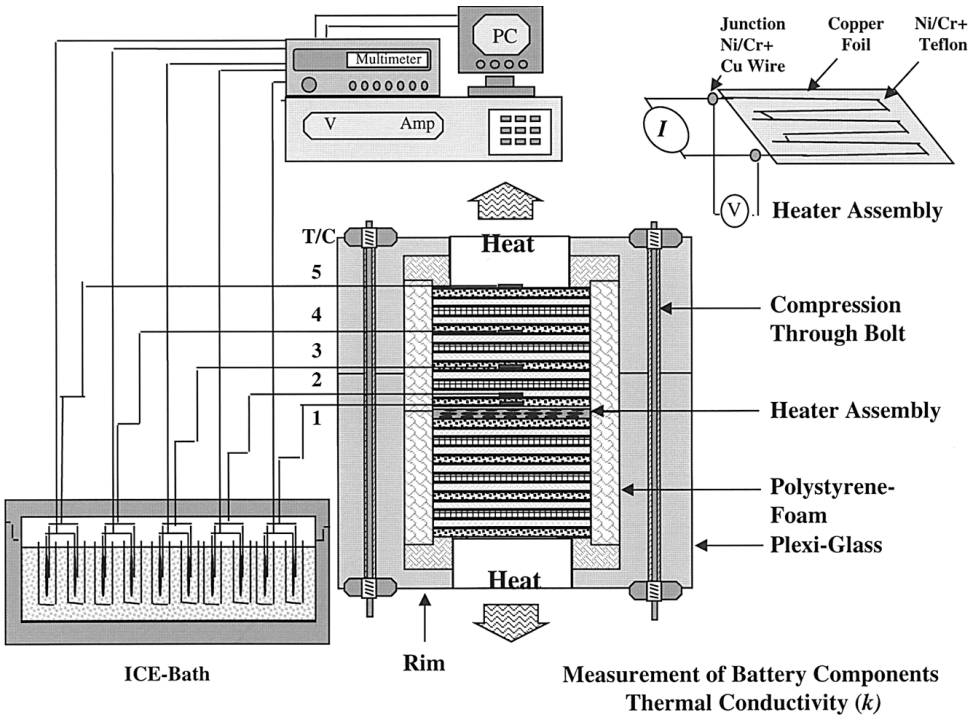

Figure 5. Schematic diagram of an experimental setup used for thermal conductivity measurement of lithium-ion battery components.

S0013-4651(98)06-095-9 CCC: $7.00

known, then the thermal conductivity may be calculated from the product of α with the effective density ρ and the effective C_p. The latter may be calculated from mass-fraction-weighted values of C_p and ρ for each component (PE, NE, and/or Sp, taken from Ref. 3 and 8) as shown in Eq. 6

$$C_p = \frac{\Sigma(\rho V C_p)_i}{\Sigma(\rho V)_i} \quad [6]$$

where V_i, ρ_i, and C_{pi} are the volume fraction, density, and specific heat capacity of the *i*th component, respectively.

The xenon flash facilities at the High Temperature Materials Laboratory (HTML) of Oak Ridge National Laboratory, Oak Ridge, TN, were used to measure the α of a stack of dissected Sony-cell components. In the XFT technique (see schematic diagram, Fig. 6a), the front face of the stack of disk-shaped samples is subjected to a short pulse of a xenon flash lamp, and the temperature rise at the rear face of the sample is measured as a function of time by a photopyrometer. Given the sample thickness (L) and half-time of the maximum temperature rise at the rear face of the sample ($t_{1/2}$), thermal diffusivity is calculated from Eq. 7

$$\alpha = 1.37\, L^2/t_{1/2} \quad [7]$$

This equation is an approximation of the unsteady-state heat conduction solution based on classical theory (see Appendix, which also has a discussion of errors associated with the method).

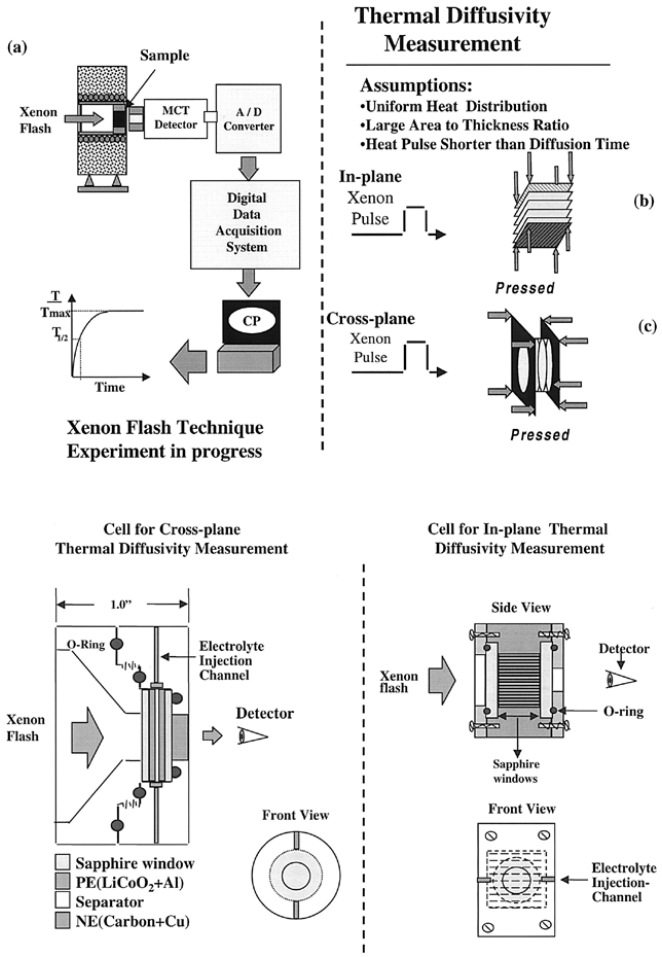

Figure 6. (a) Schematic diagram of xenon flash experimental setup; (b) arrangement of Sony 18650 cell component layers for in-plane thermal diffusivity measurement; (c) arrangement of layers for cross-plane thermal diffusivity measurement; (d) schematic diagram of the Xenon flash technique sample holders XFT arrangement designed to maintain uniform compression of stacked component layers with electrolyte.

The α of Sony-battery components PE, NE, or assemblies PE/Sp/NE were measured with and without electrolyte [1 M $LiPF_6$ in EC-DMC (1:1 wt %)], at room temperature. Two sets of α measurements were conducted: (*i*) the heat pulse was directed perpendicularly to the planar surface of disk-shaped (16 mm diam) samples of the layered components or assemblies; and (*ii*) the heat pulse was directed parallel to the planar surface of the rectangular sample layers (10 × 7 mm), stacked to form a parallelepiped of 100 mm^2 × 7 mm. The NE and PE were each 0.19 ± 0.01 mm thick, and the separator 0.020 ± 0.002 mm. Figures 6b and c show a schematic diagram of the assemblies used for cross-plane and in-plane α measurements. Both sample holders (Fig. 6d) were designed to contain electrolyte material, and the compression force was controlled such that the PE, NE, or PE/Sp/NE layers could be compressed with equal force for each individual set of measurements. This ensured the accuracy and reproducibility of the results, which requires controlled and uniform pressure over the stacked layers. Controlled compression was ensured by screwing down the two halves of the sample holder assembly until a dial gauge registered a thickness equivalent to the sum of the individually measured values of the layer and the sample holder thickness. All sample preparations for α measurements of PE, NE, or PE/Sp/NE were prepared in a glove bag filled with argon. A Sony battery, previously charged to the desired *OCV*, was dissected, and each component washed with ethanol and dried for 24 h at 65°C. Samples were cut to rectangular and disk shapes of dimensions given above and then placed in the specially designed airtight sample holders. Experiments on samples without electrolyte were conducted at first, and then they were transferred back into a glove bag for adding electrolyte. The electrolyte was injected through a small hole on the side of the sample holders, after which the hole was plugged with thermoset epoxy.

Cross-plane α measurements could be made only for a three-layer stack consisting of PE or NE, or for one PE/Sp/NE assembly. If stacks of less than three layers were used, the rear face temperature rise was too rapid and saturated the detector even when the minimum gain was used. When more than three layers were used, the signal intensity did not rise to the level needed for a reasonably accurate α value.

In our experiments, the pulse time was less than 1% of the characteristic diffusion time t_c, and the energy was uniformly absorbed at the front face of the sample. Effects of finite pulse time, nonuniform heating, and heat loss, and methods of correction for them, are discussed elsewhere.[12-16] (See also Appendix.)

Results and Discussion

Composition of electrode materials.—To determine the composition of NE and PE materials retrieved from cells at various *OCV*s (2.45 and 3.75 V), powder X-ray diffraction profiles were obtained using a diffractometer equipped with a copper target X-ray tube (Rigaku-Miniflex-CN2005C111, Rigaku Corporation, Danvers, MA). Scanning electron microscopy was used to determine the particle shape and geometry of the samples. The NE material was found to be carbon-flakes with distinct basal plane, in the size range from, 20 to 45 μm. For NE material, the intensity ratio of the (002) plane to background is R = 1.71 for *OCV* = 2.45 V, and R = 1.69 for *OCV* = 3.75 V. Based on these XRD data , it appears that the NE material is a moderate-range graphitic hard carbon, with graphene layers of lower stacking order than typical graphite. The ratio R represents the extent of the stacking of graphene layers: the stacking sequence is ABAB in the virtual absence of lithium (*OCV* = 2.45 V), and a combination of ABAB and AAAA at *OCV* = 3.75 V, corresponding to nearly complete stage 2 intercalation.

The PE material (Li_xCoO_2 particles of size 10 to 20 μm) was found to have a pronounced layer structure. The XRD profile showed a (003) to (104) plane ratio equal to 4.92.

Specific heat capacity.—Table III reports values of C_p for the Sony US-18650 lithium-ion cell. These values were measured by method 2 which, as discussed, yields more reliable results than method 1. The C_p values are 1.04 ± 0.03 J g^{-1} K^{-1} at *OCV* = 3.75 V, and 0.96 ±

S0013-4651(98)06-095-9 CCC: $7.00

0.02 J g^{-1} K^{-1} at *OCV* = 2.75 V. The C_p at *OCV* = 2.75 V agrees well with the calorimetric results reported by Haas et al.[9] (C_p = 0. 925 J g^{-1} K^{-1}). These authors provide no experimental details or information about state-of-charge of the battery.

Our results indicate that C_p increases with increase in *OCV*. In graphite, stage one lithiation causes an increase in the graphene interlayer spacing and graphene layer readjustment from ABAB to AAAA arrangement. In Li_xCoO_2, delithiation causes structural changes, which may include a phase change toward the end of charge.[18,19] This hexagonal-to-monoclinic phase change was first identified by Reimers and Dahn,[18] who detected a first-order phase transition occurring during delithiation of Li_xCoO_2. This transition involves a significant expansion of the *c* lattice parameter of the hexagonal unit cell of Li_xCoO_2. Near $x = 0.5$ this is accompanied by lattice disordering leading to a monoclinic unit cell phase transformation.[18] Tsutomu and Ueda[19] reported that delithiation of Li_xCoO_2 in the regions $0.75 < x < 1.0$ and $0 < x < 0.25$ takes place by two successive two-phase reactions, whereas in the region $0.75 < x < 0.25$ it proceeds by one single-phase reaction plus a phase change due to the formation of a monoclinic phase near $x = 0.55$. In any case, these changes are accompanied by changes of interatomic forces and distances, which are likely to affect both the phonon modes of vibrations and the electronic states near the Fermi level. These structural changes in Li_xCoO_2, caused by delithiation, may be responsible for the slight increase of C_p of the cell with *OCV*.

To analyze the behavior of C_p with *OCV* further, we note the following. The Debye temperatures (T_D) of all elemental constituents of NE and PE [Cu (340 K), C (1850 K), Al (375 K), Li (460 K), and Co (385 K)],[19] are higher than the temperature range of the present measurements (310 to 315 K). Hence, the heat capacity values are affected by the sum of contributions from electrons and phonons. An exact determination of the electron and phonon contribution to C_p, and the effect of *OCV* on this, requires knowledge of lattice vibrations and the coupling constant with the electrons, which is beyond the scope of this work. However, noting that T_D of elemental constituents of Li_xCoO_2 are much closer to the experimental temperature than that of graphite, we may at least expect that the electronic contribution to C_p of Li_xCoO_2 is smaller than that of phonons. In contrast to this, for the NE a larger electron contribution to C_p may be expected, since graphite has a high T_D (1850 K) and C_p is proportional $(T/T_D)^3$ (see Ref. 20).

The interpretation of trends in C_p values is made more difficult in the case of the NE, due to the complex nature of intercalation in graphite. When lithium ions intercalate into graphite, they share electrons with carbon-carbon rings of graphene layers in a semi-ionic bonding.[21] Thus, intercalated lithium does not exhibit a clearly ionic or clearly metallic behavior. The exact balance may depend on the type of graphitic carbon host. X-ray photoelectron spectroscopy (XPS) results by Yata et al.[12] show that lithium intercalated in hard carbon has a bond energy between 56.1 and 55.9 eV. This (1s) bond energy (ca. 56 eV) is higher by about 1 eV than that of metallic lithium (~55.2 eV), but lower than that of ionic lithium in, e.g., $LiBF_4$ (ca. 58.0 eV). Sato et al.[22] show by nuclear magnetic resonance (NMR) the presence of both ionic carbon-lithium and covalent lithium-lithium bonding in heat-treated polyphenylene. However, lithiation makes carbonaceous material an n-type host with an upshift in the Fermi level, which changes the electron energy density at the Fermi surface. This facilitates electron transfer to the conduction band in intercalated graphite and causes it to have a different electronic thermal energy than that of pure graphite. Such a condition would make the electronic contribution to heat capacity or diffusivity in the host graphite increase as the lithiation increases.

Thus, a detailed explanation of the dependence of C_p on *OCV* requires consideration of the effect of intercalation/deintercalation on the density of the vibrational modes of phonons and the electronic density of states, for both graphite and Li_xCoO_2. The data available in the literature are too scarce to allow such an analysis. However, in view of the accuracy of our measurements and based on the qualitative arguments presented above, it is not implausible that structural changes in PE and NE materials associated with the change of *OCV* = 2.75 V to *OCV* = 3.75 V cause C_p to increase from 0.96 to 1.1 J g^{-1} K^{-1}.

Thermal conductivity.—Tables IVa and IVb present cross-plane and in-plane C_p, α, and *k* values for the PE and NE components as well as PE/Sp/NE assemblies retrieved from Sony US-18650 lithium-ion batteries at *OCV* = 2.45 and 3.75 V, with and without electrolyte [1 M $LiPF_6$ in EC-DMC (1:1 wt %)].

Effect of electronic structure.—Studies reported in the literature have shown that the electrochemical properties of transition metal oxides depend on their electronic structure.[22-26] We believe that this structure, which changes with *OCV* of the lithium-ion cell, affects the thermal behavior of the materials as well. Tables IVa and IVb indicate that both cross-plane and in-plane conductivities, in the absence of electrolyte, are higher for all components of the battery at *OCV* = 3.75 V than at *OCV* = 2.45 V. In the case of the PE material, this increase may be attributed to $LiCoO_2$ being a semiconductor and becoming metallic in character upon delithiation. Molemda et al.[27]

Table IVa. Cross-plane thermal properties of Sony US-18650 lithium-ion battery components with and without electrolyte [EC-DMC (1:1 wt %)/1 M $LiPF_6$].

Materials	ρ (g cm^{-3})	C_p (J g^{-1} K^{-1})	α (cm^2 s^{-1}): sd 4 × 10^{-4}		*k* (W m^{-1} K^{-1})	
			OCV = 2.45 V	*OCV* = 3.75 V	*OCV* = 2.45 V	*OCV* = 3.75 V
PE	3.115	0.601	0.0124	0.0133	2.33	2.49
NE	1.622	0.623	0.0088	0.0119	0.89	1.20
PE/Sp/NE	2.290	1.089	0.0076	0.0095	1.90	2.36
PE/Sp/NE + electrolyte	2.680	1.280	0.0099	0.0100	3.39	3.40

Table IVb. In-plane thermal properties of Sony US-18650 lithium-ion battery components with and without electrolyte [EC-DMC (1:1 wt %)/1 M $LiPF_6$].

Materials	ρ (g cm^{-3})	C_p (J g^{-1} K^{-1})	α (cm^2 s^{-1}) *OCV* = 2.45 V	α (cm^2 s^{-1}) *OCV* = 3.75 V	*k* (W m^{-1} K^{-1}) *OCV* = 2.45 V	*k* (W m^{-1} K^{-1}) *OCV* = 3.75 V
PE	3.121	0.602	0.115 ± 0.0040	0.116 ± 0.0010	21.57	21.75
NE	1.620	0.598	0.090 ± 0.00017	0.156 ± 0.0030	8.72	15.11
PE/Sp/NE	2.291	1.088	0.0071 ± 0.0040	0.099 ± 0.00150	17.69	24.66
PE/Sp/NE + electrolyte	2.78	1.278	0.058 ± 0.0010	0.079 ± 0.0004	20.06	28.05

S0013-4651(98)06-095-9 CCC: $7.00

showed that the room-temperature electrical conductivity of $LiCoO_2$ is $\sim 10^{-3}$ S m^{-1}, increasing to $\sim 1 \times 10^2$ S m^{-1} for $Li_{0.17}CoO_2$. They stated that removing lithium ions from $LiCoO_2$ decreases the Co-Co distance. Calculations by Goodenough[28] indicate that when the Co-Co distance is less than 0.283 nm, Li_xCoO_2 has metallic character, and that it is a semiconductor when the Co-Co distance is greater than 0.283 nm. The metallic behavior is due to delocalized electrons formed when the Co-Co distance falls below the critical value. Molemda et al. point out that the Co-Co distance shrinks to about 0.281 nm as x decreases from 0.8 to 0.17. Li_xCoO_2 with $0.17 < x < 0.8$ is metallic: electrical conductivity is temperature independent. In the ranges $0.8 < x < 1$, Li_xCoO_2 is a semiconductor: electrical conductivity increases with temperature.[27] Tukomoto and West[29] attribute the $LiCoO_2$ semiconductor behavior to the presence of a small concentration of Co^{4+}. On delithiation, the Co^{4+} concentration becomes larger, and thus Li_xCoO_2 becomes metallic.

As suggested by Tsutomu and Ueda,[19] delithiation may take place via two successive two-phase reactions in the ranges $0.75 < x < 1$ and $0.25 < x < 0.75$ (the second of which in our estimation includes the PE material at $OCV = 3.75$ V), and via a single-phase reaction in the range $0 < x < 0.25$. The coexistence of two hexagonal phases having different structural parameters in Li_xCoO_2 generates delocalized electrons,[19] which contribute to C_p and to k. The increase in C_p and k values with increasing OCV may be attributed to this electron delocalization. However, the structural changes caused by delithiation also affect the phonon modes of vibration in Li_xCoO_2. This can be a reason that C_p and k of the PE material increase with OCV.

The NE material shows a much stronger increase of conductivity with OCV; at $OCV = 2.45$ V, $k = 0.89$ W m^{-1} K^{-1}, and at $OCV = 3.75$V, $k = 1.20$ W m^{-1} K^{-1}. The 26% increase within this OCV range far exceeds the increase in k of the PE, which is only about 6%. A large phonon contribution is not expected in the NE because the lattice modes are less affected by intercalation than the electronic modes. Yata et al.[12] point out that most C:Li graphitic materials are n-type semiconductors. This implies a large electronic contribution to thermal and electronic conduction. The in-plane k of the NE material is also significantly higher than the cross-plane k due to the orientation of the copper current collector (thermal conductivity 394 W m^{-1} K^{-1}) in contact with the NE material.

Effect of particle size and orientation.—According to our experience, most of the battery-grade carbon materials, except meso-carbon microbeads (MCMB) or carbon fibers, consist of flakes with a distinct basal plane. The flat planes probably become attached to each other and to the current collector during NE fabrication, in which a slurry of carbon particles in a suspension of binder and solvent is dispersed over the copper foil. The cross-plane thermal conductivity is low because the copper layers are in series with the carbon layers, and the carbon layers are deposited from the slurry such that the c axes of the flakes are oriented in the cross-plane direction. This gives the carbon layers a high thermal resistance in this direction. Electrical resistance in that direction is high as well.

Figure 7 depicts the highest heat-transfer paths in the NE, in agreement with the thermal conductivities measured in this work. The same heat-conduction paths appear to exist in the PE. There, in contrast to the NE, the in-plane thermal conductivity is expected to be only slightly higher than the cross-plane one.

Effect of electrolyte filling.—Addition of electrolyte [1 M $LiPF_6$ in EC-DMC (1:1 wt %)] significantly increases the cross-plane thermal conductivity of stacked layers of PE/Sp/NE. It practically eliminates the dependence of cross-plane conduction on OCV, but not that of in-plane conduction.

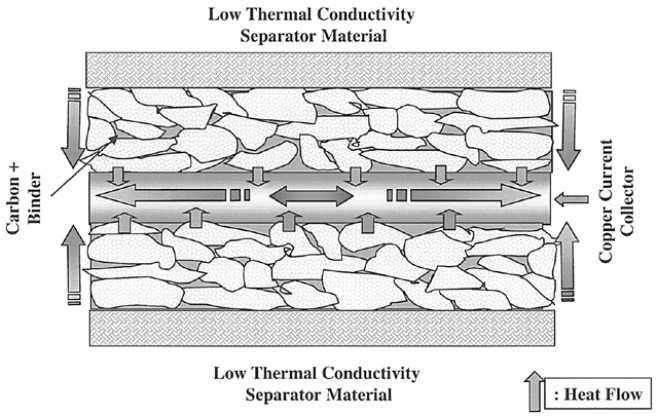

Figure 7. Schematic diagram of possible heat conduction paths in the NE of the lithium-ion battery.

Addition of electrolyte also increases the cross-plane k of stacked layers PE/Sp/NE recovered from a cell at $OCV = 2.45$ V, but only by 13%, and similarly for a cell at $OCV = 3.75$ V (Table IVb). Since the electrolyte provides good thermal contact between layers, the effect is more pronounced for the cross-plane conductivity. Table V compares the ρ, C_p, and k values of cell components from this work (at $OCV = 3.75$ V) with those reported elsewhere.[1,8] It is noteworthy that our k values, though very reproducible, deviate considerably from those of Kanari et al.[8] and are closer to those of Chen and Evans.[1] Our C_p values are lower than their values.

Conclusions

Thermal properties of the Sony US-18650 lithium-ion battery and stacked layers of components (PE, NE, or PE/Sp/NE) have been measured. The heat capacity of this battery depends on its state of charge and increases by 8% as OCV changes from 2.75 to 3.75 V. The thermal conductivity of the NE material depends more strongly on the state of charge than that of the PE material. These findings can be explained qualitatively by consideration of electronic and phonon contributions to heat capacity and thermal conductivity.

The cross-plane thermal conductivity of an electrolyte filled PE/Sp/NE assembly is 3.4 W m^{-1} K^{-1}. The in-plane thermal conductivity of stacked layers of battery components is higher than the cross-plane conductivity by nearly a factor of 10. This difference may be attributed (especially for the NE) to the orientation of particles or flakes during the formation of thin electrode layers and to the presence of the metallic current collectors.

The presence of electrolyte [1 M $LiPF_6$ in EC-DMC (1:1 wt %)] increases the thermal conductivity of the stacked layers of PE/Sp/NE by nearly 55 to 70% and eliminates the OCV dependence.

Acknowledgment

This work was supported by the Army Research Office, under grant no. DAAH04-94G-0055. The XFT facilities at Oak Ridge National Laboratory (Metals and Ceramics Division, HTML) were made available for this work with support of the University Users Program, contract DE-AC05-96OR22464 by Lockheed Martin Ener-

Table V. Thermal property values of Sony US-18650 lithium-ion battery components from this work and from the literature.

Materials	ρ (g cm^{-3})			C_p (J g^{-1} K^{-1})			k (W m^{-1} K^{-1})		
	Chen[1]	Kanari[8]	This Work	Chen	Kanari	This Work	Chen	Kanari	This Work
PE	2.920	2.810	3.115	1.134	0.849	0.601	2.18	1.29	2.49
NE	1.410	1.940	1.622	1.184	0.867	0.623	1.40	4.44	1.20

S0013-4651(98)06-095-9 CCC: $7.00

gy Research Corporation. The cooperation of Luis Revera (Merck Co. USA) in supplying electrolyte is gratefully acknowledged. The authors would like to thank Robert Zeckman (IIT Mechanical Aerospace and Materials Engineering) for technical assistance.

Appendix A

The basic theory underlying the XFT is as follows: the three-dimensional equation

$$\alpha \nabla^2 T = \frac{\partial T}{\partial t} \qquad [A\text{-}1]$$

governs heat diffusion in the sample, with temperature (T) as a function of time (t) and position (x). Assuming a finite slab of thickness L and a large area, uniformly illuminated, without heat losses at the side and back surfaces, conduction of heat becomes one-dimensional and the transient temperature is $T(x,t)$. If the input energy pulse duration is much shorter than the characteristic time of the temperature transient from the front to the back of the sample, the exact solution of Eq. A-1 may be replaced by the analytic solution for an instantaneous pulse. Parker et al.[17] have shown that the temperature rise at the rear face of the sample ($x = L$) is

$$T(L, t) = \frac{Q}{C_p \rho L}\left[1 + 2\sum_{n=1}^{\infty} (-1)^n \exp\left(\frac{-\alpha n^2 \pi^2}{L^2} t\right)\right] \qquad [A\text{-}2]$$

Here, Q is the pulse energy density (J m^{-2}) impinged on the front face of the sample; C_p the specific heat; and ρ the density of the sample. For samples less than 3 mm thick and of moderate thermal diffusivity, the pulse duration should be less than 10% of the characteristic diffusion time, which from Eq. A-2 is $t_c = L^2/\pi^2\alpha$. From Eq. A-2, the maximum temperature rise at the rear face of the sample is

$$T_{L,\max} = \frac{Q}{C_p \rho L} \qquad [A\text{-}3]$$

At any time $t > 0$, the temperature rise at the rear face of the sample as a fraction of its maximum temperature rise is

$$V = 1 + 2\sum_{n=1}^{\infty} (-1)^n \exp\left(-\frac{t}{t_c} n^2\right)$$

or [A-4]

$$V = 1 + 2\sum_{n=1}^{\infty} (-1)^n \exp(-\pi^2 n^2 B_t)$$

Here V, the normalized temperature rise, is defined as $T(L,t)/T_{L,\max}$, and $B_t = \alpha t/L^2$. From Eq. A-4 it follows that if $V_x = 1/2$, then $B_t = \alpha t/L^2 = 1.37$. Thus the half-time of the temperature rise, $t_{1/2}$, can be used to determine α

$$\alpha = 1.37 L^2/t_{1/2} \qquad [A\text{-}5]$$

Thermal diffusivity measurements by light-flash methods require accurate measurement of the effective sample thickness and the rear-face temperature rise as a function of time, at any given fraction (x) of the maximum temperature rise. Since α varies with the square of the sample thickness (L), extra attention is needed to measure the sample thickness. The uncertainties in temperature rise time on the rear face of the sample are related to deviations of the actual experimental conditions from those assumed in the mathematical models. The assumed conditions are (*i*) energy pulse time much shorter than characteristic diffusion time, (*ii*) uniform energy distribution on the front face of the sample, and (*iii*) no heat loss from the sample to the sample holder. A detailed discussion on the effects of finite pulse time, nonuniform heating, and heat-loss, as well as corrections for these, is available elsewhere.[12-17]

A major source of error is heat loss due to scattering of input light, or due to a highly reflective sample with a low aspect ratio (diameter/thickness). The method of obtaining α values used in this work is the Clark and Taylor ratio method,[13] which is independent of the heat losses. This method is based upon the difference between the theoretical no-loss curve and the normalized curve of temperature rise vs. time. Nevertheless, in this work the heat-loss effects were minimized by selecting a high-aspect-ratio design for sample geometry, using sapphire windows of high transparency to xenon light. To minimize light scattering, the sample holder and rim of the window were painted black. The opaqueness of battery components also helped minimized light scattering.

List of Symbols

A	surface area of battery or reference sample, m^2
B_t	dimensionless number for transient diffusion, Eq. A-4
C_p	heat capacity, J g^{-1} K^{-1}
h	convective heat-transfer coefficient, W m^{-2} K^{-1}
K	calorimeter constant, J K^{-1}
k	thermal conductivity, W m^{-1} K^{-1}
m	mass of cell or reference sample, kg
Q	light energy pulse density, J m^{-2}
$\dot{Q}$	heat generation rate, W
T	temperature of calorimeter or sample, K
T_a	ambient temperature, K
T_{ss}	steady-state temperature, K
t	time, s
t_c	characteristic time for diffusion, s
V	dimensionless temperature rise, Eq. A-4
V_i	volume fraction
α	thermal diffusivity, m^2 s^{-1}
ρ	effective density, kg m^{-3}
τ	dimensionless time

References

1. Y. Chen and J. W. Evans, *J. Electrochem. Soc.*,**140**, 1833 (1993).
2. Y. Chen and J. W. Evans, *J. Electrochem. Soc.*, **141**, 2947 (1994).
3. Y. Chen and J. W. Evans, *J. Electrochem. Soc.*, **143**, 2708 (1996).
4. D. Bernardi, E. Pawlikowski, and J. Newman, *J. Electrochem. Soc.*, **132**, 5 (1985).
5. C. R. Pals and J. Newman, *J. Electrochem. Soc.*, **142**, 3274 (1995).
6. C. R. Pals and J. Newman, *J. Electrochem. Soc.*, **142**, 3282 (1995).
7. J. Newman and W. Tiedemann, *J. Electrochem. Soc.*, **142**, 1054 (1995).
8. K. Kanari, K. Takano, and Y. Saito, *Bull. Electrochem. Lab*: (Umezono, Ibaraki, 305 Japan), **60**, 65 (1996).
9. O. Haas, E. Deiss, P. Novák, W. Scheifele, and A. Tuskada, in *Batteries for Portable Applications and Electric Vehicles*, C. F. Holmes and A. R. Landgrebe, Editors, PV 97-18, p. 451, The Electrochemical Society Proceedings Series, Pennington, NJ (1997).
10. J. S. Hong, H. Maleki, S. Al Hallaj, L. Redy, and J. R. Selman, *J. Electrochem. Soc.*, **145**, 1489 (1997).
11. L. J. Gibson and M. F. Ashby, *Cellular Solids Structure and Properties*, p. 201, Pergamon Press, New York (1988).
12. R. E. Taylor and K. D. Maglic, in *Compendium of Thermophysical Property Measurement Methods: Survey of Technique*, K. D. Maglic A. Cezairliyan, and V. E. Peletsky, Editors, p. 305, Plenum Press, New York (1984).
13. L. M. Clark III and R. E. Taylor, *J. Appl. Phys.*, **46**, 714 (1975).
14. M. I. Darby, S. D. Preston, and G. Whitaker, *J. Appl. Phys.*, **21**, 1146 (1988).
15. R. F. Bulmer and R. Taylor, *High Temp. High Press.*, **6**, 491 (1974).
16. Annual Book of ASTM Standard, *Standard Test Method for Thermal Diffusivity of Solids by Flash Method*, Designation: **E** 1461, ASTM, Philadelphia, PA (1992).
17. W. J. Parker, R. J. Taylor, C. P. Butler, and G. L. Abbot, *J. Appl. Phys.*, **32**, 1679 (1961).
18. J. N. Reimers and J. R. Dahn, *J. Electrochem. Soc.*, **139**, 2091 (1992).
19. T. Ohzuku and A. Ueda, *J. Electrochem. Soc.*, **141**, 2972 (1994).
20. R. E. Hummel, *Electronic Properties of Materials*, p. 269, Springer-Verlag, New York (1985).
21. S. Yata, H. Kinoshita, M. Komori, and N. Endo, *Synth. Met.*, **62**, 153 (1994).
22. K. Saito, M. Noguchi, A. Demachi, N. Oki, and M. Endo, *Science*, **264**, 556 (1994).
23. J. Braconnier, Ph.D. Thesis, University of Bordeaux I, France (1983).
24. K. Mizushima, P. C. Jones, P. J. Wiseman, and J. B. Goodenough, *Mater Res. Bull.*, **15**, 783 (1980).
25. K. Mizushima, P. C. Jones, P. J. Wiseman, and J. B. Goodenough, *Solid State Ionics*, **3/4**, 171 (1981).
26. A. Honders, J. M. Kinderen, A. H. Van Heeren, J. H. de Wit, and G. H. J. Broers, *Solid State Ionics*, **9/10**, 431 (1983).
27. J. Molenda, A. Stoklosa, and T. Bak, *Solid State Ionics*, **36**, 53 (1989).
28. J. B. Goodenough, in *Progress in Solid State Chemistry*, Vol. 5, H. Reiss, Editor, p. 279, Pergamon Press, Oxford (1986).
29. H. Tukomoto and A. R. West, *J. Electrochem. Soc.*, **144**, 3164 (1997).
30. K. Kinoshita, *Carbon: Electrochemical and Physicochemical Properties*, p. 70, Wiley, New York (1998).